Simulation of Two-Phase Flow in Models with Micro-porous Material

Vadim Lisitsa[1(✉)], Tatyana Khachkova[2], Vladislav Krutko[3], and Alexander Avdonin[3]

[1] Institute of Mathematics SB RAS, Koptug ave. 4, Novosibirsk 630090, Russia
lisitsavv@ipgg.sbras.ru
[2] Institute of Petroleum Geology and Geophysics SB RAS, Koptug ave. 3, Novosibirsk 630090, Russia
[3] Gazpromneft NTC, Moika river emb. 75-79 D, Saint-Petersburg 190000, Russia

Abstract. The paper presents an original numerical algorithm to simulate coupled two-phase fluid flow in domains containing open pores and microporous material. To simulate the coupled flow we use the time-dependent Navier-Stokes-Brinkman equation. The transport of the phases is governed by the Cahn-Hilliard equation in the open pores and by the Buckley-Leverett equation in the porous material. We suggested a unified finite-difference approximation of the two transport equations, that satisfy the natural conjugation conditions. However, Cahn-Hilliard requires an additional boundary condition, that must be satisfied at the interface to ensure the wetting angle.

Keywords: Phase-field method · flow in porous media · finite-difference simulation

1 Introduction

Pore-scale numerical simulation of fluid flow is the main application of digital rock physics (DRP). DRP allows estimating effective physical properties of rocks by numerical experiments using the micro CT-images as the rock model [3,4]. Indeed, this method can be implemented to estimate almost any property of core samples including electrical resistivity [4,19], elastic parameters such as bulk modulus or the components of the stiffness tensor [4,18,32], attenuation coefficients of seismic waves [2] and other. However, the fluid flow simulation is the most widely used application, because its results may be applied to hydrocarbon exploration, greenhouse gas sequestration as well as chemical engineering. In particular, one phase flow simulation is used to estimate absolute permeability,

T. Khachkova developed the algorithms to solve C-H and B-L equations within the FNI project FWZZ-2022-0022. V. Lisitsa performed numerical simulation using the Supercomputer of the Siant-Petersburg Polytechnical University under the support of Russian Science Foundation grant no. 21-71-20003.

© The Author(s), under exclusive license to Springer Nature Switzerland AG 2023
O. Gervasi et al. (Eds.): ICCSA 2023 Workshops, LNCS 14106, pp. 3–18, 2023.
https://doi.org/10.1007/978-3-031-37111-0_1

open porosity, and tortuosity of the pore space of the samples [4,6]. Reactive transport simulations allow understanding the peculiarities of chemical fluid-solid interaction, which may be crucial for CO_2 sequestration or CO_2 sorption [1,23,27,28,30].

Two- and multi-phase flow simulation in a pore space with complex topology is a challenging task that requires accurate numerical treatment of the moving interface. There are several approaches to resolve this issue, including direct front-tracking methods [15], level-set method [14,29], and the phase-field method [7,20,34]. The first approach is hard to implement in 3D cases, especially in domains with complex topology. The second approach allows defining the interface implicitly as the zero level of the signed distance function. It allows for treating complex geometry of the computational domain. However, it suffers from a nonphysical change of the phase volume, which requires additional regularization [17,33]. Moreover, the approximation of the wetting angle condition is also a challenging task for the level-set method. In the phase field method, the diffused interface approach is applied; i.e., the interface between the phases is smoothed out over several grid cells. It makes the concentration function smooth enough to be treated by finite differences, finite volumes, or finite elements [20]. However, an additional fourth-order differential equation called the Cahn-Hilliard equation should be solved. Due to its simplicity and applicability to the domains of almost arbitrary complexity, this approach is getting a common tool in pore-scale fluid flow simulation.

However, commonly porous materials may contain several scales of pores; i.e., the big enough pores may be filled with the microporous material which is still capable to support multi-phase flow. If a single-phase flow is considered, the coupled flow may be simulated by either explicit domain decomposition with multi-physical approaches; or by the unified Navier-Stokes-Brinkman equation [5]. However, there is no unified approach to treat the phase transport in the open pores (where the Cahn-Hilliard equation is valid) and the microporous material (where the Buckley-Leverett equation is stated). Nowadays, the widely-used approach to simulate coupled two-phase transport is based on the volume of a fluid method as reported in [10] and [11], but no coupled transport simulated with the phase-field method with the unified formulation of the Cahn-Hilliard and Buckley-Leverett equation has been published. In this paper, we present such an approach and illustrate its applicability through a series of numerical simulations in fully 3D cases.

2 Statement of the Problem

We consider the model of the rock with pores that a filled with permeable microporous material as well as open pores. We assume that the fluid flow in the open pores is governed by the Navier-Stokes equation, whereas the flow in the microporous material satisfies the Darcy law. Under this statement, we need to simulate the coupled flow of the two-phase flow of incompressible fluids. Let us introduce the computational domain $\Omega = [0; L_1] \times [0, L_2] \times [0, L_3]$ corresponding

to a CT-scan of a core. The domain is composed of three non-overlapping (multi-connected) domains Ω_s is the solid impermeable rock matrix, Ω_p is the domain filled with permeable microporous material, and Ω_o is the domain corresponding to opened pores. We also need to introduce the boundaries and interfaces. The boundary of the first type denoted as Γ_b corresponds to the sides of the computational domain $x_2 = 0$, $x_2 = L_2$, $x_3 = 0$, $x_3 = L_3$. Second, the boundaries at the inlet Γ_{in} correspond to $x_1 = 0$ and the outlet is Γ_{out} corresponding to $x_1 = L_1$. Third, the interfaces between the different types of the domains: $\Gamma_{so} = \Omega_o \cap \Omega_s$, $\Gamma_{sp} = \Omega_p \cap \Omega_s$, and $\Gamma_{po} = \Omega_o \cap \Omega_p$. The first two interfaces are impermeable, whereas the third interface supports the fluid flow.

2.1 Fluid Flow

To simulate the coupled flow we suggest using the Navier-Stokes-Brinkman equation that accounts for the free flow in the open pores and the filtration flow in the microporous material [8,10]:

$$\begin{array}{l} \frac{1}{\phi}\frac{\partial \rho \vec{v}}{\partial t} = -\nabla p + \frac{2}{\phi}\nabla \cdot (\nu \varepsilon(\vec{v})) - \kappa^{-1}\vec{v} + \vec{F}, \\ \nabla \cdot (\vec{v}) = 0. \end{array} \tag{1}$$

In these notations $\vec{v}$ is the averaged velocity vector, p is the pressure, $\varepsilon(u) = \nabla\vec{u} + \nabla\vec{u}^T$ is doubled strain tensor, $\rho = \rho(x,t)$ is fluid density depending on the particular phase, $\nu = \nu(x,t)$ is fluid viscosity, also depending on the phase, $\kappa(x,t) = \kappa_0(x)\lambda$ is the permeability with κ_0 is the absolute permeability and λ is the mobility of the fluid, depending on the saturation of particular phase, ϕ is the porosity, $\vec{F}$ is the external forces including capillary forces. In this research, we neglected the non-linear term of the Navier-Stokes equation, because the flows in porous geomaterials are slow corresponding to low Reynolds numbers. Also, we excluded the gravitational forces, because they are negligible in comparison with the capillary forces at the micro-scale.

We also need to state the boundary conditions at all the boundaries:

$$\begin{array}{ll} \vec{u} = 0, & \vec{x} \in \Gamma_b, \\ \vec{u} = 0, & \vec{x} \in \Gamma_{so}, \\ \vec{u} = 0, & \vec{x} \in \Gamma_{sp}, \\ \vec{u} \cdot \vec{n} = U_0, & \vec{x} \in \Gamma_{in}, \\ \vec{u} \cdot \vec{\tau_1} = 0, & \vec{x} \in \Gamma_{in}, \\ \vec{u} \cdot \vec{\tau_2} = 0, & \vec{x} \in \Gamma_{in}, \\ p = P_0, & \vec{x} \in \Gamma_{out}, \end{array} \tag{2}$$

where $\vec{n}$ is a vector normal to the interface pointing inward to Ω, and $\vec{\tau}_j$ are two the tangential vectors. The first three conditions are no-flow conditions at the sides of the domain, and at the interfaces between the pores (either open or filled with microporous material) and the impermeable rock matrix. The last three conditions are stated at the inlet and outlet to support the fluid flow. Continuity of the velocity and pressure at the interface Γ_{op}; i.e., between the open and filled pores are satisfied implicitly by the Navier-Stokes-Brinkmann equation. The initial conditions are assumed to be zero.

2.2 Phase Transport in Open Pores

To simulate the phase transport in open pores we use the phase-field model [12,13,20]:

$$\begin{array}{l} \frac{\partial \psi}{\partial t} + \vec{u} \cdot \nabla \psi = \nabla \cdot (M(\psi) \nabla \mu), \\ \mu = F'(\psi) - \varepsilon^2 \Delta \psi, \end{array} \tag{3}$$

where $\psi \in [0,1]$ - is the order parameter defining the phase. The potential $F(\psi)$ is defined as

$$F'(\psi) = 2\psi(\psi-1)(2\psi-1).$$

This is the fourth-order in space differential equation, thus boundary value problem requires two boundary conditions at each boundary:

$$\begin{array}{ll} \nabla \mu \cdot \vec{n} = 0, \nabla \psi \cdot \vec{n} = -\frac{\sqrt{2}}{\varepsilon}(\psi^2 - \psi)\cos(\theta), & \vec{x} \in \Gamma_b \cup \Gamma_{so}, \\ \nabla \mu \cdot \vec{n} = 0, \nabla \psi \cdot \vec{n} = 0, & \vec{x} \in \Gamma_{out}, \\ \nabla \mu \cdot \vec{n} = 0, \psi = \Psi_{in}, & \vec{x} \in \Gamma_{in}. \end{array} \tag{4}$$

The first set of conditions are stated at the impermeable boundaries, and enforce the wetting angle equal to θ, which is measured for phase one; i.e., $\psi = 1$, see [16,21] for the details. The condition at the outlet allows the free outward transport of the phase. The third condition defines the distribution of the phases at the inlet. Note, that the condition at the interface Γ_{op} is missing. It is the subject of this research and it will be clarified below.

2.3 Transport in the Microporous Media

Transport of the two-phase fluid in porous media satisfies the Buckley-Leverett equation, typically written for the wetting phase:

$$\phi \frac{\partial S}{\partial t} + \nabla \cdot \left(\frac{\lambda_1(S)}{\lambda(S)} \vec{u} \right) + \nabla \cdot \left(\kappa \frac{\lambda_1(S)\lambda_0(S)}{\lambda(S)} \frac{dp_{01}}{dS} \nabla S \right) = 0. \tag{5}$$

where S is a saturation of the first (wetting) phase, $S \in [0,1]$. Parameters $\lambda_j = \kappa_{rj}/\nu_j$, are mobilities of the corresponding phases, total mobility is $\lambda = \lambda_0 + \lambda_1$, κ_{rj} is the relative permeability of phase j, which depends on the saturation, and ν_j is the viscosity of the phase j. Parameter p_{01} is the pressure difference between phases 0 and 1. The equation is stated in the domain Ω_p that is in the pores filled with microporous material. We need to state the boundary conditions:

$$\begin{array}{ll} \nabla S \cdot \vec{n} = 0, & \vec{x} \in \Gamma_b, \\ \nabla S \cdot \vec{n} = 0, & \vec{x} \in \Gamma_{out}, \\ \nabla S \cdot \vec{n} = 0, & \vec{x} \in \Gamma_{ps}, \\ S = S_0, & \vec{x} \in \Gamma_{in}. \end{array} \tag{6}$$

Same as before the conditions at Γ_{po} are required, which will be specified below.

Coefficients of Eq. (5) depend on the saturation. In this work, we use the following model. First, we assume that the saturation is bounded by the residual

saturation of each phase: $S \in [S_{r1}, 1 - S_{r0}]$. Note, that if the saturation equals S_{r1} the flow will transport only phase 1, thus only this phase will flow away from the microporous material. The same is valid for phase 0. The construct the equations of state we need to introduce the normalized saturation as:

$$S_j^N = \frac{1 - S_{jr}}{1 - S_{1r} - S_{2r}}. \tag{7}$$

After that, the relative permeability and the capillary pressure can be defined as:

$$\kappa_{jr} = \kappa_{jr}^{max}(S_j^N)^{a_j} \tag{8}$$

$$p_{01} = P_{c0}(S_1^N)^{-c}, \tag{9}$$

where κ_{jr}^{max} is the maximal phase permeability of the considered phase, P_{c0} reference pressure which may depend on the absolute permeability and porosity. Parameters a_j and c are chosen to match lab measurements.

3 Conjugation Conditions

Above, we described the models which are used to simulate the fluid flow and phase transport in open pores and the pores filled with a microporous permeable material. However, the goal of this research is to combine the model, to simulate coupled transport of the two-phase fluid.

Consider Cahn-Hilliard Eq. (3) and the Buckley-Leverett Eq. (5) and rewrite them in pseudo divergence-free form:

$$\begin{aligned} &\phi\tfrac{\partial q}{\partial t} + \nabla \cdot (f(q)\vec{u}) - \nabla \cdot (D(q)\nabla\mu) = 0, \\ &\mu(x < 0) = F'(q) - \varepsilon^2 \Delta q, \\ &\mu(x > 0) = q, \end{aligned} \tag{10}$$

where q represents either the normalized saturation S^N for the Buckley-Leverett equation or the order parameter ψ for the Cahn-Hilliard equation. The coefficients of the equation can be represented as follows:

$$f(q) = \begin{cases} q, & x < 0 \\ \lambda_1(q)/\lambda(q), & x > 0 \end{cases} \tag{11}$$

$$D(q) = \begin{cases} M(q), & x < 0 \\ -\kappa\frac{\lambda_1(S)\lambda_2(S)}{\lambda(S)}\frac{dp_{21}}{dS}, & x > 0 \end{cases} \tag{12}$$

$$\mu(q) = \begin{cases} F'(q) - \varepsilon^2 \Delta q, & x < 0 \\ q, & x > 0 \end{cases} \tag{13}$$

After that we may construct the conjugation conditions by introducing a closed contour containing the interface, integrating over the volume, and using the divergence theorem. This leads to the following conditions:

$$[f(q)] = 0, [D\tfrac{\partial \mu}{\partial n}] = 0.$$

The relations can be reformulated in the original notations as

$$\psi|_{0-} = \lambda_1(S)/\lambda(S)|_{0+},\ M\frac{\partial \mu}{\partial x}|_{0-} = -\kappa\frac{\lambda_1(S)\lambda_2(S)}{\lambda(S)}\frac{dp_{21}}{dS}\frac{\partial S}{\partial x}|_{0+}.$$

Note, that the Cahn-Hillard equation contains the fourth-order in space differential operator, thus additional equation is needed to close the problem:

$$\frac{\partial \psi}{\partial n} = -\frac{\sqrt{2}}{\varepsilon}(\psi^2 - \psi)\cos(\theta)|_{0-}. \tag{14}$$

This condition ensures the proper wetting angle of the fluid 1 at the surface Γ_{op}.

4 Numerical Scheme

To solve the coupled system of Eqs. (1), (3), and (5) we use the finite difference schemes on staggered grids, where pressure p_{i_1,i_2,i_3}, saturation S_{i_1,i_2,i_3}, order parameter ψ_{i_1,i_2,i_3}, and chemical potential μ_{i_1,i_2,i_3} are defined in integer grid points $(x_j)_{i_j} = h_j i_j$, where $j = 1, 2, 3$ and h_j is the grid step along x_j direction. Components of the velocity vector are stored in half-integer points in one spatial direction; i.e., $(v_1)_{i_1+1/2,i_2,i_3}$, $(v_2)_{i_1,i_2+1/2,i_3}$, $(v_1)_{i_1,i_2,i_3+1/2}$. After that, we applied the splitting technique to construct an almost explicit in time finite difference approximation of the entire problem.

Assume the solution is known up to the instant $t = t^n = n\tau$, where τ is the time step. We fix the coefficients of the Navier-Stokes-Brinkman equation:

$$\begin{gathered}\rho^n_{i_1,i_2,i_3} = q^n_{i_1,i_2,i_3}\rho_1 + (1 - q^n_{i_1,i_2,i_3})\rho_0,\\ \nu^n_{i_1,i_2,i_3} = (q^n_{i_1,i_2,i_3}\nu_1^{-1} + (1 - q^n_{i_1,i_2,i_3})\nu_0^{-1})^{-1},\\ \kappa^n_{i_1,i_2,i_3} = \kappa^0\lambda(q^n_{i_1,i_2,i_3}),\end{gathered} \tag{15}$$

where $q = \psi$ for $\vec{x} \in \Omega_o$, and $q = S^N$ for $\vec{x} \in \Omega_p$. Note, that density and permeability are defined in the integer points, whereas the Navier-Stokes-Brinkman equations are approximated in the half-integer points along one direction. Thus, we need further modify them using the arithmetic averaging over two adjoin integer points; i.e., $\rho^n_{i_1+1/2,i_2,i_3} = 0.5(\rho^n_{i_1+1,i_2,i_3} + \rho^n_{i_1,i_2,i_3})$, see [22,31] for the details.

4.1 Approximation of Navier-Stokes-Brinkman Equation

To solve the Navier-Stokes-Brinkman equation we use the projection-type scheme [9] with the further splitting of the Navier-Stokes and Brinkman terms:

$$\begin{gathered}\frac{\rho^n}{\phi}\frac{\vec{u}^* - \vec{u}^n}{\tau} = \frac{2}{\phi}\nabla_h \cdot (\mu^n \varepsilon_h(\vec{u}^n)) + \vec{F}^n,\\ \frac{\rho^n}{\phi}\frac{\vec{u}^{**} - \vec{u}^*}{\tau} = -(k^n)^{-1}\vec{u}^{**},\\ \frac{\rho^n}{\phi}\frac{\vec{u}^{n+1} - \vec{u}^{**}}{\tau} = -\nabla_h p^{n+1},\\ \nabla_h \cdot \vec{u}^{n+1} = 0,\end{gathered} \tag{16}$$

We omit the subscripts (i_1, i_2, i_3) in these equations, but use the notations ∇_h and ε_h to point out that the finite-difference operators, approximating the differential ones are used. Note, that the second equation, corresponding to the Brinkman term is approximated by the implicit scheme because the explicit one requires unacceptably small time stepping. The last two equations lead to the projection step which requires solving the Poisson equation for the pressure field. We use the Krylov-type iterative method with the original pseudo-spectral preconditioner to solve it [19]. The finite-difference operators approximating the spatial derivatives are second-order two-point central differences, and the approximation of the time derivatives is first-order accurate.

4.2 Approximation of Cahn-Hilliard Equation and the Buckley-Leverett Equation

Consider Eq. (10) representing the phase transport in a general form. We use the same staggered grid scheme to approximate it. We define the phase and the chemical potential in the integer grid points and the velocity components are stored in half-integer points. To approximate the advection term, one may use either upwind or WENO scheme [24,30]. The diffusion term may be approximated using the second-order central differences. Also, the Laplacian in the equation for the chemical potential is approximated with the second order. In general, we use explicit in time scheme:

$$\begin{aligned} &\phi\tfrac{q^{n+1}-q^n}{\tau} + \nabla_u \cdot (f(q^n)\vec{u}^{n+1}) - \nabla_h \cdot (D(q^n)\nabla_h \mu^n) = 0, \\ &\mu^n(x<0) = F'(q^n) - \varepsilon^2 \Delta_h q^n, \\ &\mu^n(x>0) = q^n. \end{aligned} \tag{17}$$

To approximate the boundary conditions< mainly the non-linear condition for the wetting angle, we use immersed boundary method [26].

4.3 Approximation of the Conjugation Conditions

To approximate the conjugation conditions, we do not need to consider them explicitly. Instead, we use the finite-difference approximation 17 throughout the entire computational domain $\Omega_o \cup \Omega_p$ with the coefficients defined according to formulae (11)–(13). However, the definition of the chemical potential μ inside the domain Ω_o requires evaluation of the Laplacian of the phase variable. Thus, an extra boundary condition has to be satisfied. We use the wetting-angle boundary condition (14) and approximate it using immersed boundary method [26] at the interface Γ_{op}.

5 Numerical Experiments

5.1 A Droplet on an Impermeable Surface

The first series of experiments was done to validate the algorithm. We considered a computational domain Ω being a cube with the side of $2 \cdot 10^{-4}$ m. The side

of the cube $x_1 = 0$ was the inlet, and the side $x_1 = 2 \cdot 10^{-4}$ was the outlets. The other four sides were impermeable. We placed an impermeable barrier for $x_1 \in [4 \cdot 10^{-5}, 6 \cdot 10^{-5}]$ m. The pressure difference between the inlet and outlet was equal to zero, i.e., no external flow was assumed. After that, we stated the initial conditions. We considered two types of initial conditions. First, phase 1 occupies the domain Ω_o except for the droplet of phase 0 which was a hemisphere of the radius of $4 \cdot 10^{-5}$ m, centered in point $(8 \cdot 10^{-5}, \cdot 10^{-4}, \cdot 10^{-4})$. Second, we performed the opposite situation; i.e., a droplet of phase 1 with a background of phase 0. In all our experiments we assume phase 1 is the wetting phase and measure the wetting angle with respect to it so that the wetting angle is always less than 90°. The other parameters of the fluids were fixed as provided in the Table 1. The simulations were done using the spatial steps equal to $2 \cdot 10^{-6}$ m. Thus the radius of the original droplet was only 20 grid points. We simulated the evolution of the droplet at the flat surface, which turned into a part of a sphere with a radius depending on the wetting angle. We measured the form of the droplet and the pressure drop according to estimates, presented in [25]. If the original droplet was a semi-sphere of radius R_0, the curvature radius of the final droplet will be

$$R_f = R_0 \left(\frac{2}{2 - 3\cos(\phi) + \cos^3(\phi)} \right)^{1/3}.$$

and the pressure difference is

$$\Delta P = \frac{2\sigma}{R_f},$$

where ϕ is the wetting angle.

Theoretical estimation of the pressure difference inside and outside of the droplet for different wetting angles are presented in Table 2. Note, that the error in pressure estimation may reach up to 5% for wetting angles between 30° and 120°, but it may approach 7% for small wetting angles. In our opinion, this may be caused by poor resolution of the droplet, especially taking into account the size of the droplet in comparison with the interfacial tension. To illustrate the solution to the considered problems, we provide 2D cross-sections of the solution corresponding to the wetting angles of 60° and 120° in Fig. 1. Additionally, we plot the sectors of the sphere, that the droplet suppose to form, and the lines corresponding to the considered wetting angles to illustrate a good agreement of the experiments with the theoretical estimates.

Table 1. Fluid parameters.

	Phase 1	Phase 0
viscosity, ν (Pa/s)	$3.8 \cdot 10^{-4}$	$4.027 \cdot 10^{-3}$
mass density, ρ (kg/m^3)	1000	880
interfacial tension σ_{10} N/m	$2.571 \cdot 10^{-2}$	

Table 2. Theoretical estimation (ΔP_t) and simulations results (ΔP_e) of the pressure difference inside and outside of the droplet placed at a flat surface for different wetting angles.

angle	R_f (m)	ΔP_t (Pa)	ΔP_e (Pa)	angle	R_f (m)	ΔP_t (Pa)	ΔP_e (Pa)
20	$22.8 \cdot 10^{-5}$	224.8	219	160	$3.18 \cdot 10^{-5}$	1618.2	1703
25	$11.7 \cdot 10^{-5}$	300.4	295	155	$3.18 \cdot 10^{-5}$	1616.2	1701
30	$13.5 \cdot 10^{-5}$	379.5	376	150	$3.19 \cdot 10^{-5}$	1612.7	1697
35	$11.2 \cdot 10^{-5}$	460.9	461	145	$3.20 \cdot 10^{-5}$	1607.1	1693
40	$9.46 \cdot 10^{-5}$	543.8	547	140	$3.22 \cdot 10^{-5}$	1598.9	1690
45	$8.20 \cdot 10^{-5}$	627.1	633	135	$3.24 \cdot 10^{-5}$	1587.7	1680
50	$7.24 \cdot 10^{-5}$	710.2	719	130	$3.27 \cdot 10^{-5}$	1572.8	1658
55	$6.49 \cdot 10^{-5}$	792.1	805	125	$3.31 \cdot 10^{-5}$	1553.8	1633
60	$5.89 \cdot 10^{-5}$	872.3	889	120	$3.36 \cdot 10^{-5}$	1530.5	1607
65	$5.41 \cdot 10^{-5}$	950.2	971	115	$3.42 \cdot 10^{-5}$	1502.3	1574
70	$5.02 \cdot 10^{-5}$	1025.0	1049	110	$3.50 \cdot 10^{-5}$	1469.2	1533
75	$4.69 \cdot 10^{-5}$	1096.4	1126	105	$3.59 \cdot 10^{-5}$	1431.0	1493
80	$4.42 \cdot 10^{-5}$	1163.9	1198	100	$3.71 \cdot 10^{-5}$	1387.7	1439
85	$4.19 \cdot 10^{-5}$	1227.0	1266	95	$3.84 \cdot 10^{-5}$	1339.1	1384

5.2 A Droplet on a Porous Surface

The second series of experiments was done for the droplet placed on the flat surface of porous material. We used the results of the previous simulations with formed droplets with proper wetting angles as the initial conditions. The size of the domain and the grid steps were the same as before. We changed the impermeable barrier for $x_1 \in [4 \cdot 10^{-5}, 6 \cdot 10^{-5}]$ m to the homogeneous porous material with porosity equal to 0.1 and absolute permeability $\kappa_0 = 10^{-13}\ m^2$ which is approximately 0.1 Darcy. The parameters of the Buckley-Leverett model are provided in Table 3. The pressure difference between the inlet and outlet was equal to zero. Model time was $1.35 \cdot 10^{-3}$ s. Note, that the initial saturation of the porous material was S_{1r} if the background was filled with phase 0, and $1 - S_{0r}$ if the background corresponded to phase 1.

Table 3. Parameters of the Buckley-Leverett model.

	Phase 1	Phase 0
k_{jr}^{max}	0.31	0.91
a_j	2.585	1.552
S_{jr}	0.38	0.26
P_0	$9 \cdot 10^4$	
c	0.246	

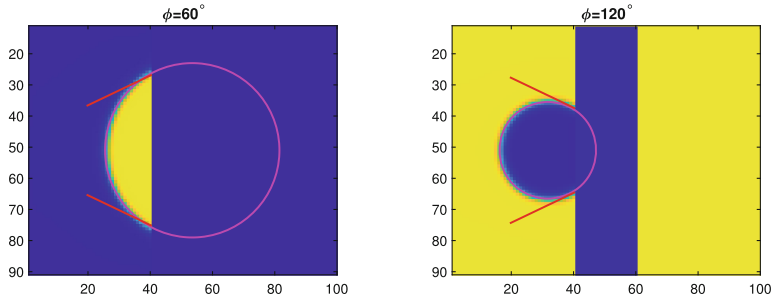

Fig. 1. 2D cross-sections of the droplets on an impermeable surface corresponding to wetting angles equal to 60° (left) and 120° (right). The circle represents the cross-section of the theoretically predicted droplet shape. The inclination of the lines corresponds to the wetting angles. Axes are in grid points.

In Figs. 2 and 3 we provide snapshots of the solution at different time instants for the models with the wetting angle 60° and 120°, respectively. If the fluid of the droplet is a wetting phase, the porous material starts absorbing the droplet, due to the capillary forces. Note, that the droplet preserves the shape and the wetting angles whereas its volume is reduced. This is due to the use of static wetting angles in the conjugation conditions. When the droplet of the non-wetting phase is considered (Fig. 3) some fluid starts to saturate the porous material at the very first instants. This is happening due to the pressure difference inside and outside of the droplet. However, the capillary pressure in the porous material growing with saturation and equilibrates the external force. As a result the droplet slightly reduces in size but preserves the shape and wetting angles.

5.3 A Droplet on a Porous Surface with External Flow

The third series of experiments are done for the same setup as the previous one. However, we added a positive pressure drop between the inlet and outlet, so that $\Delta P = 10^5$ Pa. In this case, the average fluid flow velocity in the x_1 direction was 0.1 m/s. Simulation time was $1.35 \cdot 10^{-3}$ s, thus approximately half of the pore volume was injected. The snapshots with wetting and non-wetting droplet are presented in Figs. 4 and 5 respectively.

If a droplet of wetting fluid is considered, the filtration process is fast, so that the snapshots are presented at earlier instants, than in all other considered cases. Note, that the wetting fluid tends to saturate the porous material and only a relatively small part of it flows out. Moreover, the non-wetting phase flowing out of the porous material start forming a droplet inside the wetting phase until the wetting phase breaks away. The volume of the bubble of the wetting phase is much smaller than that at the initial stage because it is partially locked by the capillary forces inside the porous material. An opposite situation is observed if the non-wetting phase forms a droplet on the porous material. The non-wetting phase is forced to filtrate through the porous layer. Almost no diffusive spreading

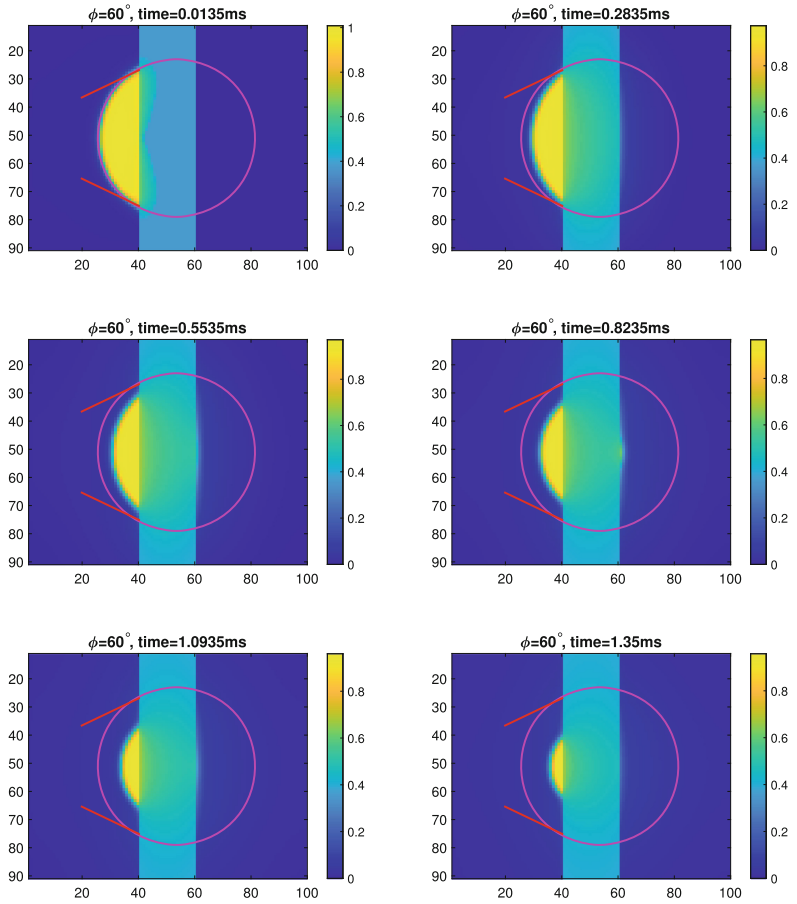

Fig. 2. 2D cross-sections of the droplets on a porous barrier corresponding to wetting angles equal to 60° at different time instants. The circle represents the cross-section of the theoretically predicted droplet shape on an impermeable surface.

of the non-wetting phase is observed in tangential directions inside the porous layer so the external flow is the major transport factor. When breaks through the porous layer, the non-wetting phase forms a spherical bubble, opposite to the filtration of the wetting phase.

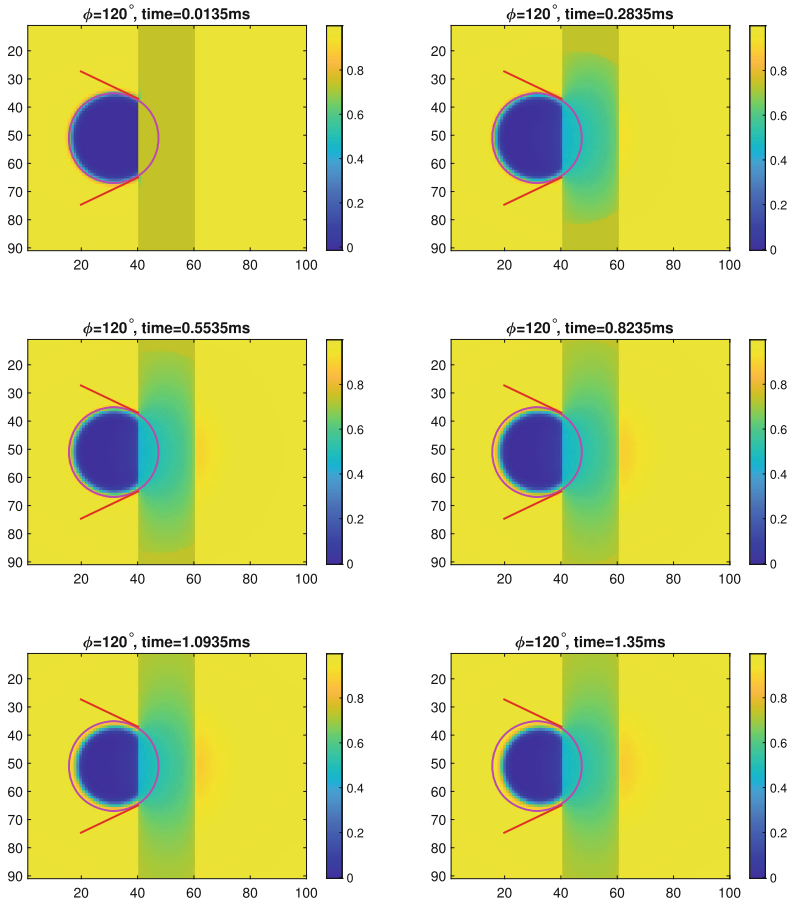

Fig. 3. 2D cross-sections of the droplets on a porous barrier corresponding to wetting angles equal to 120° at different time instants. The circle represents the cross-section of the theoretically predicted droplet shape on an impermeable surface.

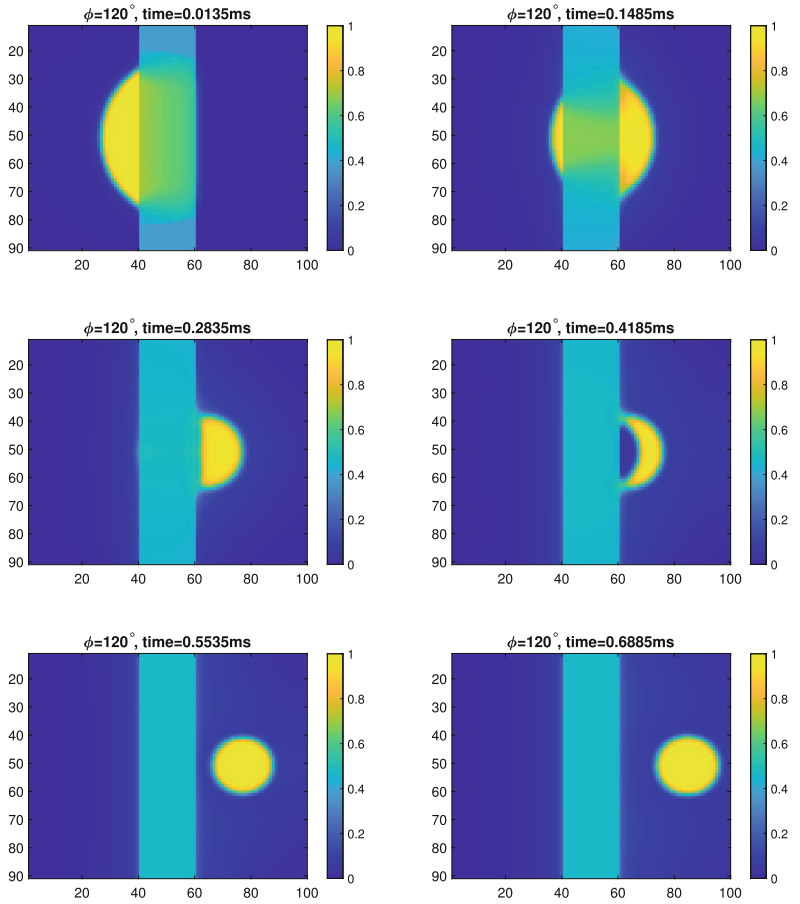

Fig. 4. 2D cross-sections of the droplets on a porous barrier corresponding to wetting angles equal to 60° at different time instants. Experiment with the external flow.

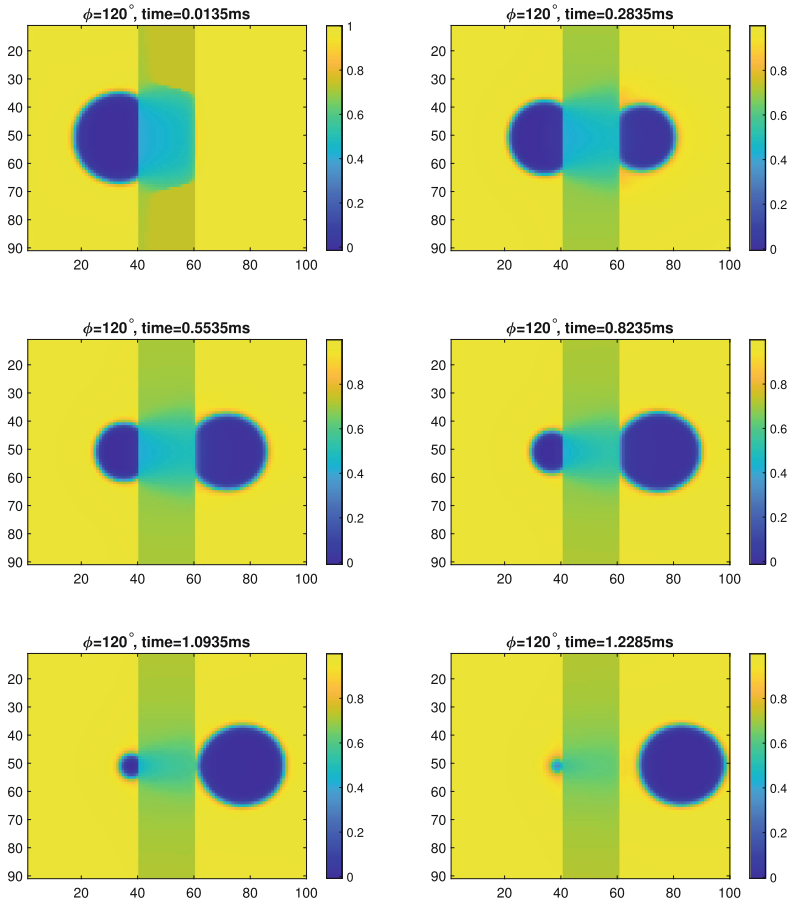

Fig. 5. 2D cross-sections of the droplets on a porous barrier corresponding to wetting angles equal to 120° at different time instants. Experiment with the external flow.

6 Conclusion

We presented an original numerical algorithm to simulate coupled two-phase fluid flow in domains containing open pores and microporous material. Free flow is simulated in the open pores and the Darcy filtration flow is assumed in the microporous subdomains. To simulate the coupled flow we used the time-dependent Navier-Stokes-Brinkman equation. The transport of the phases is governed by the Cahn-Hilliard equation in the open pores and by the Buckley-Leverett equation in the porous material. We suggested a unified finite-difference approximation of the two transport equations, that satisfy the natural conjugation conditions. However, Cahn-Hilliard requires an additional boundary condition, that must be satisfied at the interface to ensure the wetting angle. The derived coupled system is approximated by the finite-differences

with the explicit approximation of the Navier-Stokes equation and Cahn-Hilliard-Buckley-Leverett equations. However, an implicit approximation of the Brinkman part is applied. The algorithm is implemented in 3D using CUDA technology. According to the presented numerical experiments the algorithm is capable of simulating the saturation of the porous materials and breaking one phase through the porous material, forming droplets after breaking away.

References

1. Al-Khulaifi, Y., Lin, Q., Blunt, M.J., Bijeljic, B.: Pore-scale dissolution by CO_2 saturated brine in a multimineral carbonate at reservoir conditions: impact of physical and chemical heterogeneity. Water Resour. Res. **55**(4), 3171–3193 (2019)
2. Alkhimenkov, Y., et al.: Frequency-dependent attenuation and dispersion caused by squirt flow: three-dimensional numerical study. Geophysics **85**(3), MR129–MR145 (2020)
3. Andra, H., et al.: Digital rock physics benchmarks - part I: imaging and segmentation. Comput. Geosci. **50**, 25–32 (2013)
4. Andra, H., et al.: Digital rock physics benchmarks - part II: computing effective properties. Comput. Geosci. **50**, 33–43 (2013)
5. Nillama, L.B.A., Yang, J., Yang, L.: An explicit stabilised finite element method for navier-stokes-brinkman equations. J. Comput. Phys. **457**, 111033 (2022). https://doi.org/10.1016/j.jcp.2022.111033
6. Bazaikin, Y., et al.: Effect of CT image size and resolution on the accuracy of rock property estimates. J. Geophys. Res.: Solid Earth **122**(5), 3635–3647 (2017)
7. Boyer, F., Lapuerta, C., Minjeaud, S., Piar, B., Quintard, M.: Cahn-Hilliard/Navier-stokes model for the simulation of three-phase flows. Transp. Porous Media **82**(3), 463–483 (2010)
8. Brinkman, H.C.: A calculation of the viscous force exerted by a flowing fluid on a dense swarm of particles. J. Appl. Sci. Res. **A1**, 27–34 (1947)
9. Brown, D.L., Cortez, R., Minion, M.L.: Accurate projection methods for the incompressible Navier-stokes equations. J. Comput. Phys. **168**(2), 464–499 (2001)
10. Carrillo, F.J., Bourg, I.C., Soulaine, C.: Multiphase flow modeling in multiscale porous media: an open-source micro-continuum approach. J. Comput. Phys.: X **8**, 100073 (2020)
11. Carrillo, F.J., Soulaine, C., Bourg, I.C.: The impact of sub-resolution porosity on numerical simulations of multiphase flow. Adv. Water Resour. **161**, 104094 (2022)
12. Chen, J., Sun, S., Chen, Z.: Coupling two-phase fluid flow with two-phase darcy flow in anisotropic porous media. Adv. Mech. Eng. **6**, 871021 (2014). https://doi.org/10.1155/2014/871021
13. Chen, L., Zhao, J.: A novel second-order linear scheme for the Cahn-Hilliard-Navier-stokes equations. J. Comput. Phys. **423**, 109782 (2020). https://doi.org/10.1016/j.jcp.2020.109782
14. Gibou, F., Fedkiw, R., Osher, S.: A review of level-set methods and some recent applications. J. Comput. Phys. **353**, 82–109 (2018)
15. Groot, R.D.: Second order front tracking algorithm for Stefan problem on a regular grid. J. Comput. Phys. **372**, 956–971 (2018). https://doi.org/10.1016/j.jcp.2018.04.051
16. Jacqmin, D.: Contact-line dynamics of a diffuse fluid interface. J. Fluid Mech. **402**, 57–88 (2000)

17. Jettestuen, E., Friis, H.A., Helland, J.O.: A locally conservative multiphase level set method for capillary-controlled displacements in porous media. J. Comput. Phys. **428**, 109965 (2021). https://doi.org/10.1016/j.jcp.2020.109965
18. Khachkova, T., Lisitsa, V., Kolyukhin, D., Reshetova, G.: Influence of interfaces roughness on elastic properties of layered media. Probab. Eng. Mech. **66**, 103170 (2021)
19. Khachkova, T., Lisitsa, V., Reshetova, G., Tcheverda, V.: GPU-based algorithm for evaluating the electrical resistivity of digital rocks. Comput. Math. Appl. **82**, 200–211 (2021)
20. Kim, J.: Phase-field models for multi-component fluid flows. Commun. Computat. Phys. **12**(3), 613–661 (2012)
21. Lacis, U., et al.: Steady moving contact line of water over a no-slip substrate. Eur. Phys. J. Spec. Top. **229**(10), 1897–1921 (2020)
22. Lisitsa, V., Podgornova, O., Tcheverda, V.: On the interface error analysis for finite difference wave simulation. Comput. Geosci. **14**(4), 769–778 (2010)
23. Lisitsa, V., Bazaikin, Y., Khachkova, T.: Computational topology-based characterization of pore space changes due to chemical dissolution of rocks. Appl. Math. Model. **88**, 21–37 (2020). https://doi.org/10.1016/j.apm.2020.06.037
24. Luo, K., Zhuang, Z., Fan, J., Haugen, N.E.L.: A ghost-cell immersed boundary method for simulations of heat transfer in compressible flows under different boundary conditions. Int. J. Heat Mass Transf. **92**, 708–717 (2016)
25. Mirsandi, H., Rajkotwala, A.H., Baltussen, M.W., Peters, E.A.J.F., Kuipers, J.A.M.: Numerical simulation of bubble formation with a moving contact line using local front reconstruction method. Chem. Eng. Sci. **187**, 415–431 (2018)
26. Mittal, R., Iaccarino, G.: Immersed boundary methods. Annu. Rev. Fluid Mech. **37**(1), 239–261 (2005)
27. Molins, S., Trebotich, D., Steefel, C.I., Shen, C.: An investigation of the effect of pore scale flow on average geochemical reaction rates using direct numerical simulation. Water Resour. Res. **48**(3), W03527 (2012)
28. Molins, S., et al.: Pore-scale controls on calcite dissolution rates from flow-through laboratory and numerical experiments. Environ. Sci. Technol. **48**(13), 7453–7460 (2014)
29. Osher, S., Fedkiw, R.P.: Level set methods: an overview and some recent results. J. Comput. Phys. **169**(2), 463–502 (2001)
30. Prokhorov, D., Lisitsa, V., Khachkova, T., Bazaikin, Y., Yang, Y.: Topology-based characterization of chemically-induced pore space changes using reduction of 3d digital images. J. Comput. Sci. **58**, 101550 (2022)
31. Samarskii, A.A.: The Theory of Difference Schemes, Pure and Applied Mathematics, vol. 240. CRC Press, Boca Raton (2001)
32. Shulakova, V., et al.: Computational elastic up-scaling of sandstone on the basis of x-ray micro-tomographic images. Geophys. Prospect. **61**(2), 287–301 (2013)
33. Sussman, M., Fatemi, E.: An efficient, interface-preserving level set redistancing algorithm and its application to interfacial incompressible fluid flow. SIAM J. Sci. Comput. **20**(4), 1165–1191 (1999)
34. Yang, J., Kim, J.: A novel Cahn-Hilliard-Navier-stokes model with a nonstandard variable mobility for two-phase incompressible fluid flow. Comput. Fluids **213**, 104755 (2020). https://doi.org/10.1016/j.compfluid.2020.104755